

A UNIFIED CONSTITUTIVE MODEL OF HAYNES 230 FOR FATIGUE-CREEP BEHAVIOR UNDER LONG-TERM HOLDING AT HIGH TEMPERATURES

Rou Du¹, Hengxu Song¹, Qiang Li², Qiang Liu², Nan Li², Xiaoming Liu¹

¹ LNM, Institute of Mechanics, Chinese Academy of Sciences, Beijing 100190, China (durou@imech.ac.cn)

² China Institute of Atomic Energy, Beijing 102413, China

ABSTRACT

Haynes 230 alloy is a promising structural material for nuclear reactors due to its outstanding mechanical properties at high temperatures. These include creep strength, oxidation resistance, and cyclic strength. Assessing the structural integrity of Haynes 230 involves inelastic analysis, crucially dependent on developing a robust constitutive model that accurately depicts the complex deformation responses under operational conditions. In this study, we introduced a macroscopic constitutive model to characterize the isothermal fatigue-creep behavior of Haynes 230, especially under prolonged holding times. We developed a viscoplastic model within the unified Chaboche framework, enhancing the kinematic hardening rule to encompass the intricate aspects of static recovery in Haynes 230. This model successfully captures both fatigue and stress relaxation behaviors at temperatures ranging from 750°C to 850°C, with holding times of 10 and 30 minutes, respectively. We employed a Bayesian inference approach for parameter determination in the constitutive model. This approach involved two steps: (i) creating a Gaussian Process surrogate model using data from finite element method simulations, and (ii) parameter estimation using Markov Chain Monte Carlo sampling within the Bayesian framework. Results indicate that our developed constitutive model precisely replicates the fatigue-creep responses of Haynes 230 across various temperatures and holding times.

INTRODUCTION

The advancement of sophisticated structural alloys, designed to endure extreme conditions, is crucial for high-temperature applications like nuclear reactors. Haynes 230, in particular, stands out among potential candidates, garnering significant interest for its extraordinary mechanical properties at high temperatures. These properties encompass exceptional creep strength, oxidation resistance, and cyclic strength. Assessing the structural integrity of Haynes 230 is vital for its deployment in challenging environments. This assessment demands comprehensive inelastic analysis, a cornerstone of which is the development of a robust constitutive model. Such a model is essential to precisely depict the complex deformation behaviors of the alloy under various operational conditions.

In the past few decades, the development of inelastic constitutive models has been pivotal in simulating fatigue-creep interactions in alloys that deform under high-temperature conditions. These models are broadly classified into two categories: unified and non-unified. The unified constitutive model, noted for its proficiency in effectively describing fatigue-creep interactions, has been the subject of extensive research. A key feature of this model is the kinematic hardening rule, which typically incorporates elements of linear hardening, dynamic recovery, and static recovery. These components collectively enhance the model's capability to accurately represent the complex mechanical behavior of alloys under stress. The first two terms are responsible for capturing the strain- or stress-controlled cyclic behaviours without dwell (Kang, 2004). Meanwhile, the static recovery term is utilized to replicate the effect of holding time on cyclic behaviours (Ramaswamy et al., 1990; Chaboche, 2008). For example, Yaguchi et al. (2002) employed the static recovery term to describe the creep and stress relaxation-induced increase of mean stress. Additionally, Zhan and Tong (2007) demonstrated that the static recovery term in the modified Chaboche model could predict the stress relaxation behaviours of the nickel-based superalloy at various cyclic strain rates. More recently, Ahmed et al. (2016) improved the visco-plastic model by incorporating the effect the strain range and rate on the fatigue creep interaction of the Haynes 230 alloy. While the unified constitutive model demonstrates high accuracy

for short holding periods, its suitability diminishes for longer durations due to the absence of a time-dependent physical mechanism. Additionally, the interdependence of static recovery parameters complicates their determination via traditional trial-and-error methods.

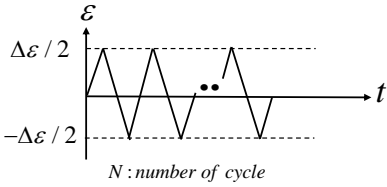
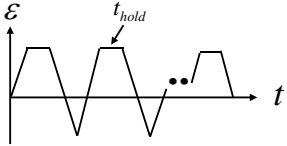
Addressing this limitation, our paper presents a macroscopic constitutive model specifically tailored to capture the complex isothermal fatigue-creep behaviors of Haynes 230 during extended holding times. This model is formulated within the unified Chaboche framework, incorporating a modified kinematic hardening rule to better represent the unique static recovery characteristics of Haynes 230. To accurately determine the parameters of the static recovery term, we utilize the Bayesian inference method in a sequential two-step approach. The efficacy of this model is validated through its application to fatigue and stress relaxation responses at temperatures ranging from 750°C to 850°C and holding times of 10 and 30 minutes. This demonstrates the model's ability to effectively simulate the material's behavior under varying thermal and temporal conditions.

EXPERIMENTAL STUDY

Materials and testing conditions

In this study, Haynes 230 nickel alloy was selected. To characterize the cyclic mechanical behaviour under elevated temperatures, we machined the specimen into a solid bar. The machined specimen exhibits a section diameter of 6 mm and gauge length of 36 mm. The testing conditions are displayed in Table 1. All high-temperature tests were conducted using the Materials Testing Systems servo-hydraulic test machine. The testing temperature ranged from 750 °C to 850 °C.

Table 1: Summary of experimental conditions under elevated temperatures

Experimental type	Testing condition	Schematic diagram
Low Cycle Fatigue (LCF)	$\diamond \dot{\epsilon} = 10^{-3} \text{ s}^{-1}, \Delta\epsilon / 2 = 0.5 \%$ $N = 200$ $T = 750^\circ\text{C}, 800^\circ\text{C}, 850^\circ\text{C}$	 <p style="text-align: center;">N: number of cycle</p>
Fatigue Creep Interaction (FCI)	$\diamond \dot{\epsilon} = 10^{-3} \text{ s}^{-1}, \Delta\epsilon / 2 = 0.5 \%$ $N = 200$ $T = 750^\circ\text{C}, 800^\circ\text{C}, 850^\circ\text{C}$ $t_{hold} = 10 \text{ min}, 30 \text{ min}$	

Experimental results

To illustrate the stress-strain responses of Haynes 230 under various testing conditions, we establish the following parameters within the stress-strain hysteresis curve, as depicted in Figure 1. Points S and E denote the start and end of the dwell-period. Consequently, the stress relaxation ($\Delta\sigma_r$) is determined as the difference between the stresses at S and E . The maximum stress (σ_{\max}) and minimum stress (σ_{\min}) refer to the peak point and valley point in the loop, respectively. The stress amplitude (σ_{xa}) and mean stress (σ_{xm}) are defined by:

$$\sigma_{xa} = (\sigma_{\max} - \sigma_{\min}) / 2 \quad (1)$$

$$\sigma_{xm} = (\sigma_{\max} + \sigma_{\min}) / 2 \quad (2)$$

This formulation allows for a comprehensive analysis of the stress-strain behaviour under different conditions.

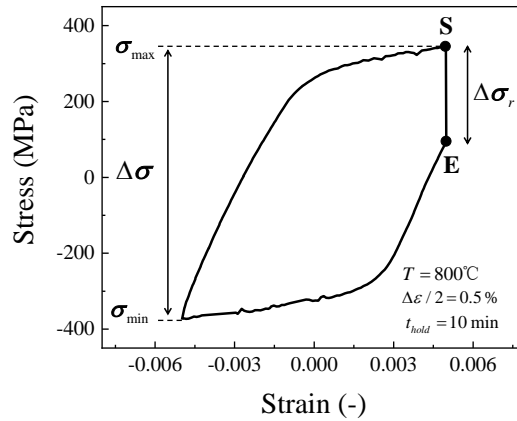


Figure 1. Defined parameters in the typical stress-strain hysteresis curve to qualify mechanical responses

(a) Low Cycle Fatigue (LCF) tests

The low cycle fatigue (LCF) test was performed at a strain rate of $1 \times 10^{-3} \text{ s}^{-1}$ with a selected strain amplitude $\Delta\varepsilon / 2$ of 0.5%. As depicted in Figure 2, the mean stress was maintained at zero for all the testing temperatures. Furthermore, the material exhibited an initial cyclic hardening and reached a saturated state after certain loading cycle. Nevertheless, the saturated stress displayed a decrease with rising temperatures.

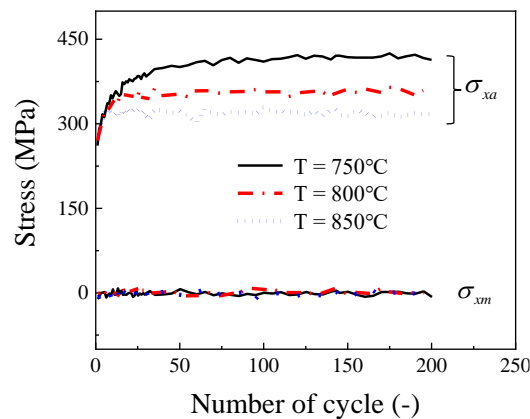


Figure 2. Low cycle fatigue tests at different testing temperatures: evolution of stress amplitude and mean stress with loading cycles

(b) Fatigue Creep Interaction (FCI) tests

For the fatigue creep interaction (FCI) test, the testing conditions were identical to those of the low cycle fatigue (LCF) test, except for the addition holding time at the maximum strain. Specifically, two holding time, 10min and 30min, were selected.

The experimental results are presented in Figure 3. Generally, the holding time exhibited limited influence on the evolution of stress amplitude across the three testing temperatures, even the material exhibits a little cyclic softening after 50 cycles at the temperature of 850 °C. Also, the mean stress decrease at 750 °C and 800 °C with the cycle. Another feature of the FIC test referred to the evolution of the stress relaxation. Shown in Figure 3(c), the stress relaxation increases with loading cycles and testing temperatures up to 50 cycles. However, at 850 °C, the stress relaxation started to decrease after 50 cycles, a phenomenon attributed to the cyclic softening (Barrett et al., 2016). Furthermore, the holding time was observed to increase stress relaxation during the initial loading cycles; nevertheless, beyond 100 cycles, the holding time exhibited no discernible impact on stress relaxation.

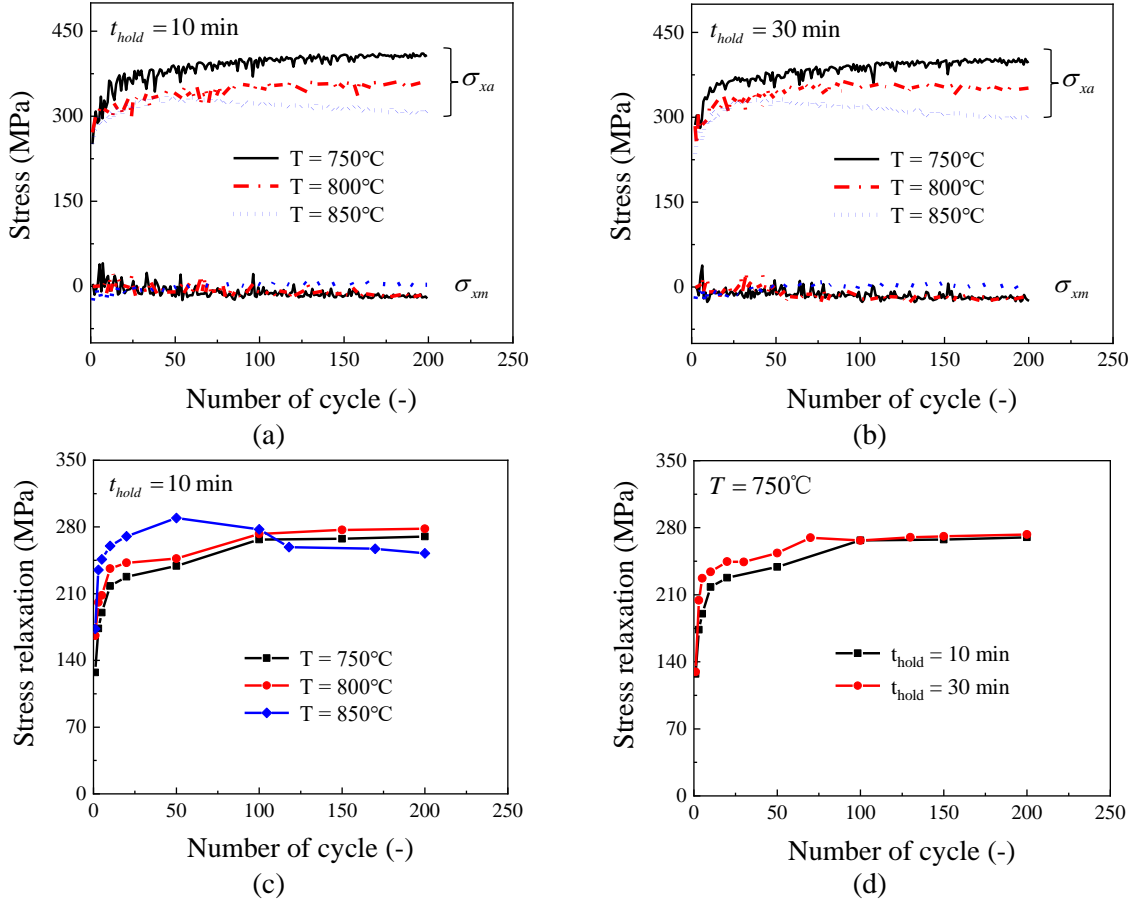


Figure 3. Fatigue creep interaction tests: (a) evolution of stress amplitude and mean stress for holding time of 10 min, and (b) 30 min; (c) stress relaxation for 10 min holding at different temperatures; (d) stress relaxation at 750 °C for different holding times.

CONSTITUTIVE MODELLING

Brief explanation of the constitutive model

The constitutive model employed in this study is in the framework of unified Chaboche model, under the assumption of small strain isotropic elasticity:

$$\boldsymbol{\varepsilon} = \boldsymbol{\varepsilon}^e + \boldsymbol{\varepsilon}^{in} \quad (3)$$

$$\boldsymbol{\varepsilon}^e = \mathbf{D}^{-1} : \boldsymbol{\sigma} \quad (4)$$

$$\dot{\boldsymbol{\varepsilon}}^{in} = \sqrt{\frac{3}{2}} \left\langle \frac{F}{K} \right\rangle^n \frac{s - \boldsymbol{\alpha}}{|s - \boldsymbol{\alpha}|} \quad (5)$$

$$F = \sqrt{\frac{3}{2} (s - \boldsymbol{\alpha}) : (s - \boldsymbol{\alpha})} - \sigma_0 \quad (6)$$

where \mathbf{D} , s and $\boldsymbol{\alpha}$ represent the elastic tensor, the deviatoric stress tensor and the back stress tensor, respectively. σ_0 means the initial yield stress. K and n are material parameters. $\langle \cdot \rangle$ is Macauley bracket, which means $\langle x \rangle = 0$ when $x < 0$ and $\langle x \rangle = x$ when $x \geq 0$.

Based on the experimental results for Haynes 230 at each temperature, three key characterizations emerge:

- Absence of isotropic hardening. During the cyclic loading, the yield stress remains constant, indicating the absence of isotropic hardening.

- Variation of plastic modulus with loading cycles. The plastic modulus undergoes changes as the cycles progress under cyclic loading conditions.
- Time dependency in cyclic holding period. Time plays a significant role during the cycling holding period, implying time-dependent behavior in the material response.

Building upon the observed experimental characteristics, only kinematic hardening rule is included in the constitutive model. Specifically, the kinematic hardening rule in this investigation comprises the following three terms (Du et al., 2023):

$$\boldsymbol{\alpha} = \sum_{i=1}^M \boldsymbol{\alpha}_i \quad (7)$$

$$\dot{\boldsymbol{\alpha}}_i = \frac{2}{3} C_i(p) \dot{\boldsymbol{\epsilon}}_p - \xi_i \boldsymbol{\alpha}_i \dot{p} - r(p, t_{relax}) [J(\boldsymbol{\alpha}_i)]^{m-1} \boldsymbol{\alpha}_i \quad (8)$$

where \dot{p} is the equivalent inelastic strain rate, $J(\boldsymbol{\alpha}_i)$ is the second invariant of back stress; C_i and ξ_i are material parameters related to the linear hardening term and the dynamic recovery term, respectively; r and m are the parameters in the static recovery term. Different from the classical Chaboche model, the parameter C_i ($i=1,2$) is set as the function of accumulated plastic strain, while r as the function of accumulated plastic strain and relaxation time:

$$C_i(p) = C_i^0 + C_i^\Delta [1 - \exp(-D_i p)] \quad (9)$$

$$r(p, t_{relax}) = r_0 [\varphi_s + (1 - \varphi_s) e^{-(\omega_1 p + \omega_2 t_{relax})}] \quad (10)$$

where C_i^0 , C_i^Δ and D_i are parameters to control the shapes of hysteresis curves; r_0 , φ_s , ω_1 and ω_2 are parameters simulate the cyclic relaxation behaviours; p is the accumulated plastic strain. The form of Equation (10) was initially introduced by Zhang and Xuan (2017) considering solely the influence of accumulated plastic strain. In our previous study, we extended this formulation by incorporating the mechanism of static recovery during strain holding period, thereby integrating the relaxation time into the static recovery item (Du et al., 2023). It is essential to highlight that the parameters in Equation (10) are coupled with each other, and difficult to be identified analytically.

Parameters' calibration

Within this section, the parameters of the constitutive model will be calibrated separately at three distinct testing temperatures. Following the identification approach, these parameters fall into two classes, as shown in Table 2. The first class encompasses parameters that can be obtained 'directly' through the extraction or fitting of the experimental data. In contrast, the second class involves parameters within highly non-linear equations or demonstrating high correlations. Consequently, the identification of these parameters requires more sophisticated or 'advanced' methods.

Table 2 Classification of parameters in the constitutive model

	Item	Parameter
First Class	Visco-plastic	K, n
	Elastic	E, ν, σ_0
	Kinematic hardening (besides static recovery)	$C_1^0, C_2^0, C_3, \xi_1, \xi_2, \xi_3,$ $C_1^\Delta, C_2^\Delta, D_1, D_2$
	Kinematic (with static recovery)	$r_0, \varphi_s, \omega_1, \omega_2, m$

(a) Parameters in the first class

As the identification for the parameters in the first class is simple, we only present a concise overview of the calibration procedure. Initially, the rate-dependent parameter K and n are obtained by fitting the uniaxial tensile stress-strain curves. Subsequently, the parameters associated with hardening rules, excluding the static recovery, are calibrated using the low cycle fatigue test. Specifically, these parameters are determined by analysing the hysteresis shape for both the initial and final cycles.

(b) Parameters in the second class

The parameters in the second class are related to the static recovery term within the hardening rule. In contrast to the parameters in the first class, the parameters in the second class exhibit high correlations within the constitutive equation, making them challenging to identify through conventional trial-and-error methods. Although Zhang and Xuan (2017) successfully employed this conventional method, it was limited to a restricted number of parameters. Therefore, we adopt an advanced parameter identification approach: Bayesian inverse method.

The fundamental concept behind the Bayesian inverse method is to derive the posterior Probability Density Function (PDF) of parameters by integrating the initial belief with the likelihood function, which can be calculated by experimental results. However, obtaining the posterior PDF analytically in real-world data proves challenging. To address this issue, an approximate method named Markov Chain Monte Carlo (MCMC) is often employed. Generally, the MCMC method requires the order of samples to be $10^4 - 10^6$ to ensure the stationary distribution of the Markov chain (Betancourt, 2017). Unfortunately, constructing such a database directly through finite element simulations is computationally infeasible. As an alternative, we use the Gaussian process surrogate model to substitute the results from finite element simulations. The detailed theory of Gaussian process surrogate model and Bayesian inference approach can be referred to our previous work (Du et al., 2023).

Therefore, to calibrate kinematic hardening parameters (r_0 , φ_s , ω_1 , ω_2 and m) in second class, we use the Bayesian inverse method by the following two steps: (i) establishing a Gaussian Process surrogate model by using the data generated from the finite element method, and (ii) obtaining the value of parameters by using Markov Chain Monte Carlo sampling under the Bayesian framework. For the first step, the desired dataset comprises a total of 2401 FE simulations, where the four parameters are selected in the ranges of $-7.0 \leq \log(r_0) \leq -5.0$, $1.0 \leq \log(\varphi_s) \leq 2.0$, $-3.0 \leq \log(\omega_2) \leq -1.0$ and $2.5 \leq m \leq 4.0$ with a uniform distribution. The parameter ω_1 is fixed to be 0.04, which can simulate the inflection point in the relaxed stress curves. Therefore, the datasets for constructing the GP surrogated model consist of the input $\mathbf{X} = (\log(r_0), \log(\varphi_s), \log(\omega_2), m)$ and the output $\mathbf{Y} = (\sigma^{ij})$, where σ^{ij} represents the relaxed stress at the different relaxed times $t_{relax} = [0 \text{ s}, 600 \text{ s}]$ with an interval of 30 s in the loading cycles. Here, we select the cyclic number $N = 1, 10, 50, \text{ and } 200$, as those cycles effectively capture the stress relaxation behaviours. Using the datasets generated by the FE simulations, the GP surrogate model is trained using the GPytorch package. Additionally, an extra set of 500 FE simulations is performed as the test data to assess the effectiveness of the surrogate model.

For the second step, we use the MCMC sampling to calculate the PDF of those four parameters. For the prior PDF of the four parameters, we adopt the uniform distributions within the selected ranges. Applying Bayes' theorem, we can compute the PDF of parameters \mathbf{X} by:

$$P(\mathbf{X} | \sigma_{pred}^{i,j}) = \frac{P(\sigma_{pred}^{i,j} | \mathbf{X})P(\mathbf{X})}{P(\sigma_{pred}^{i,j})} \quad (11)$$

where $P(\sigma_{pred}^{i,j})$ is the marginalized posterior for predicted relaxed stress. By using the above equation with the MCMC sampling, the PDF of parameters $\log(r_0)$, $\log(\varphi_s)$, $\log(\omega_2)$ and m can be obtained. The values corresponding to the maximum probability density are then selected as the inferred parameters.

All the identified parameters related to the kinematic hardening at three testing temperatures are listed in Table 3. Due to the reason of project, the parameters related to the visco-plastic and elastic items are not presented.

Table 3: Identified parameters of the constitutive model

T/°C	C_1^0	C_2^0	C_3	ξ_1	ξ_2	ξ_3	C_1^Δ	C_2^Δ
750	146708.1	12684.9	9500.0	6743.5	731.9	70.0	666103.8	32632.4
800	146708.1	12684.9	9500.0	6743.5	731.9	70.0	418921.6	11073.8
850	146708.1	12684.9	9500.0	6743.5	731.9	70.0	198176.2	64000.4
T/°C	D_1	D_2	r_0	φ_s	ω_1	ω_2	m	
750	5.0	7.0	7.06×10^{-7}	88.3	0.04	0.092	3.348	
800	10.0	14.0	1.92×10^{-6}	44.15	0.04	0.02	3.306	
850	15.0	20.0	2.16×10^{-6}	15.3	0.04	0.0015	3.288	

Verification of the constitutive model's predictability

After obtaining the parameters of the constitutive model at each temperature, we assess the model's predictability by comparing the results between simulations and experiments.

(a) Low cycle fatigue tests

The parameters related to low cycle fatigue has been identified by fitting the evolution of stress amplitude and shapes of stress-strain hysterical curves. Figure 4 demonstrates that the calibrated constitutive model accurately describes these experimental results.

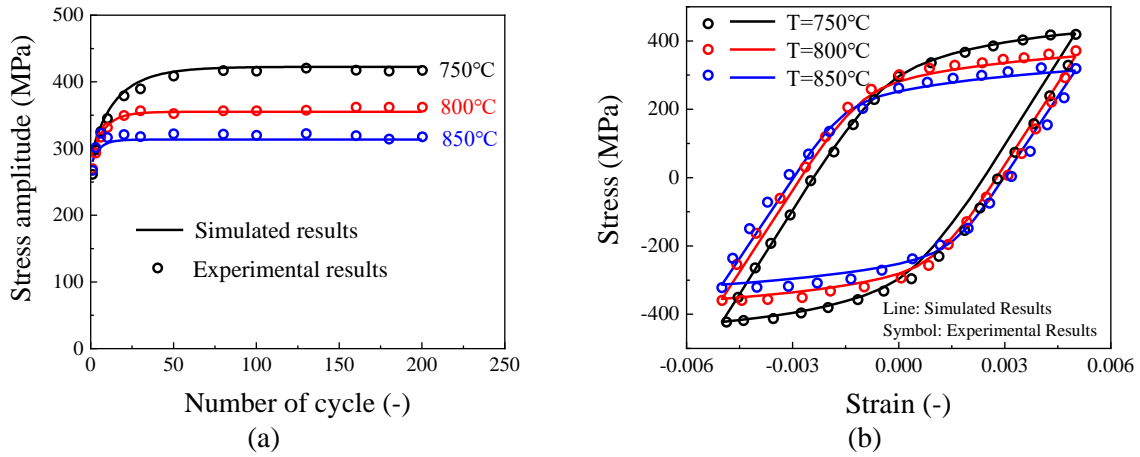


Figure 4. Comparison between simulations and experiments for low cycle fatigue tests: (a) evolution of stress amplitude with loading cycles; (b) stress-strain hysterical curves at 200th cycle.

(b) Fatigue creep interaction tests

We conduct a comparison between simulated and experimental results for the stress amplitude evolution and hysterical curves at 200th cycle in FCI tests. As illustrated in Figure 5, the predict stress amplitude shows a slight deviation from the experimental results during the initial cycles, but this difference diminishes with an increasing number of loading cycle. Additionally, the hysterical curves at 200th cycle are precisely predicted by the numerical results. Figure 6 further demonstrates the comparison of stress relaxation for typical loading cycles, affirming the predictability of the identified constitutive model for the cyclic relaxation behaviours. Overall, the model provides a reliable representation of the experimental observations in the context of fatigue creep interaction.

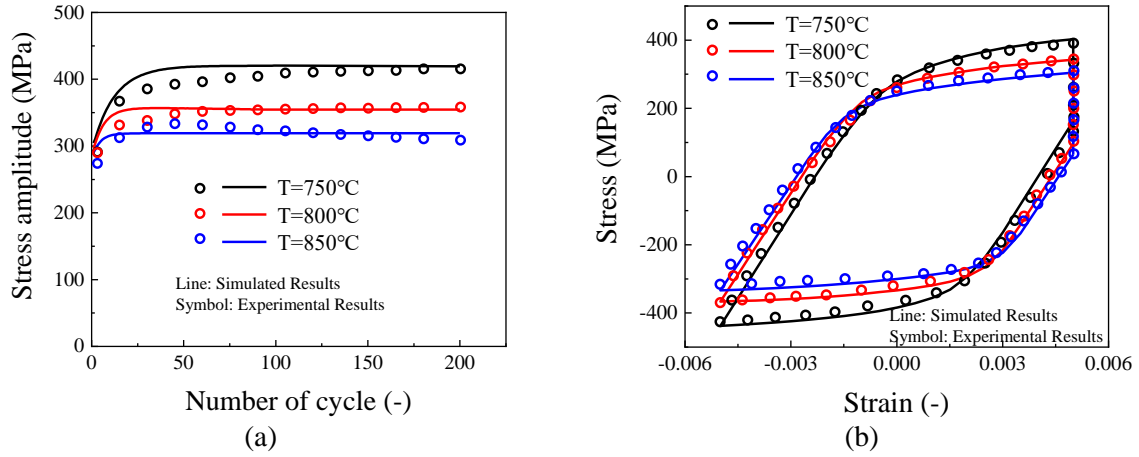


Figure 5. Comparison between simulations and experiments for fatigue creep interaction tests: (a) evolution of stress amplitude with loading cycles; (b) stress-strain hysterical curves at 200th cycle.

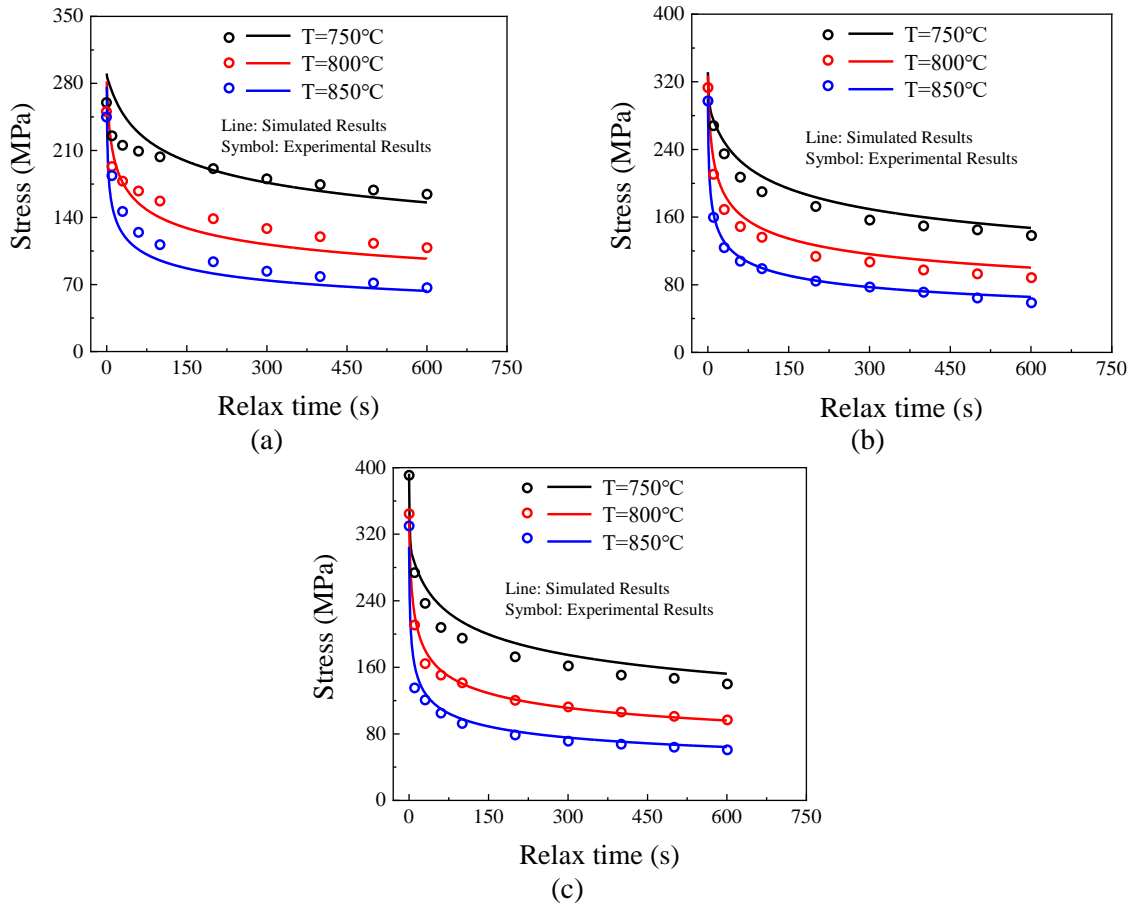


Figure 6. Comparison between simulations and experiments for fatigue creep interaction tests for different loading cycle: (a) N = 1; (b) N = 10; (c) N=200

In summary, the calibration of the constitutive model's parameters, achieved through a combination of fitting processes and the Bayesian inverse method, significantly enhances its ability to accurately describe cyclic loading behaviors at various temperatures, encompassing scenarios both with and without strain holding. This comprehensive calibration approach substantially improves the model's predictive accuracy and robustness under diverse conditions. Such advancements contribute to a more reliable and precise representation of material responses under cyclic loading, which is crucial for predicting the performance and lifespan of materials used in high-stress, high-temperature environments like nuclear reactors.

CONCLUSION

In this research, we present a unified constitutive model, developed within the Chaboche framework, to describe the cyclic behaviors of Haynes 230 alloy at high temperatures. Our experimental findings indicate that this material exhibits initial cyclic hardening, eventually reaching a state of saturation after a certain number of loading cycles in both Low Cycle Fatigue (LCF) and Fatigue Creep Interaction (FCI) tests. Notably, the experiments also show that while holding time leads to increased stress relaxation in the initial cycles, it has a relatively minimal impact on the stress amplitude's evolution.

To accurately simulate these observed cyclic behaviors, we have integrated the concepts of relaxation time and accumulated plastic strain into the static recovery term of the kinematic hardening rule. This integration is critical in capturing the nuanced mechanical responses of the alloy, particularly under varying conditions of temperature and loading.

The application of the Bayesian inverse method for parameter identification has been a key aspect of our approach. This method has enabled our constitutive model to effectively replicate the fatigue-creep responses of Haynes 230 under a range of temperature conditions and holding times. Our model's ability to mirror these complex responses not only underscores its accuracy and robustness but also significantly contributes to the broader understanding of the mechanical behaviors of this alloy. Ultimately, this study advances the methodologies for modelling cyclic behaviors in Haynes 230, offering valuable insights for the application of this alloy in high-temperature environments.

REFERENCES

- Ahmed, R., Barrett, P.R., Hassan, T., 2016. Unified viscoplasticity modeling for isothermal low-cycle fatigue and fatigue-creep stress-strain responses of Haynes 230. *Int. J. Solids Struct.* 88–89, 131–145. <https://doi.org/10.1016/j.ijsolstr.2016.03.012>
- Barrett, P.R., Ahmed, R., Menon, M., Hassan, T., 2016. Isothermal low-cycle fatigue and fatigue-creep of Haynes 230. *Int. J. Solids Struct.* 88–89, 146–164. <https://doi.org/10.1016/j.ijsolstr.2016.03.011>
- Betancourt, M., 2017. A conceptual introduction to Hamiltonian Monte Carlo. *ArXiv Prepr. ArXiv170102434*.
- Chaboche, J.L., 2008. A review of some plasticity and viscoplasticity constitutive theories. *Int. J. Plast.* 24, 1642–1693. <https://doi.org/10.1016/j.ijplas.2008.03.009>
- Du, R., Song, H., Gao, F., Mo, Y., Yan, Z., Zhuang, Z., Liu, X., Wei, Y., 2023. Machine learning informed visco-plastic model for the cyclic relaxation of 316H stainless steel at 550°C. *Int. J. Plast.* 103743. <https://doi.org/10.1016/j.ijplas.2023.103743>
- Kang, G., 2004. A visco-plastic constitutive model for ratcheting of cyclically stable materials and its Finite element implementation. *Mech. Mater.* 14.
- Ramaswamy, V.G., Stouffer, D.C., Laflen, J.H., 1990. A Unified Constitutive Model for the Inelastic Uniaxial Response of Rene' 80 at Temperatures Between 538C and 982C. *J. Eng. Mater. Technol.* 112, 280–286. <https://doi.org/10.1115/1.2903324>
- Yaguchi, M., Yamamoto, M., Ogata, T., 2002. A viscoplastic constitutive model for nickel-base superalloy, part I: kinematic hardening rule of anisotropic dynamic recovery. *Int. J. Plast.* 18, 1083–1109. [https://doi.org/10.1016/S0749-6419\(01\)00029-8](https://doi.org/10.1016/S0749-6419(01)00029-8)
- Zhan, Z.-L., Tong, J., 2007. A study of cyclic plasticity and viscoplasticity in a new nickel-based superalloy using unified constitutive equations. Part II: Simulation of cyclic stress relaxation. *Mech. Mater.* 39, 73–80. <https://doi.org/10.1016/j.mechmat.2006.01.006>
- Zhang, S.-L., Xuan, F.-Z., 2017. Interaction of cyclic softening and stress relaxation of 9–12% Cr steel under strain-controlled fatigue-creep condition: Experimental and modeling. *Int. J. Plast.* 98, 45–64. <https://doi.org/10.1016/j.ijplas.2017.06.007>